JOURNAL OF CATALYSIS 32, 452–465 (1974)

The Kinetics of Hydrogen Peroxide Decomposition Catalyzed by Cobalt–Iron Oxides

J. R. GOLDSTEIN AND A. C. C. TSEUNG

Department of Chemistry, The City University, St. John Street, London EC1V 4PB

Received April 9, 1973

The kinetics, in alkaline solution, of heterogeneous H_2O_2 decomposition by the cobalt–iron spinel oxide system, $Co_xFe_{3-x}O_4$, $(0 \leq x \leq 3)$, were studied with a view to defining the intrinsic and microstructural factors influencing the catalytic activity. The activity order for two catalyst series, prepared by hydroxide and oxalate co-precipitation routes, was found to be (considering x values)

$$1.0 > 1.5 > 2.0 > 2.4 > 3.0 > 0.6 > 0.0$$

on the basis of diffusion-free activation energies for the decomposition reaction. This order agreed with results obtained by measuring the initial rates of H_2O_2 decomposition, provided the rates were normalized for the available area of reaction at the catalyst surface. The activity order can be interpreted in terms of the electronic structure of cobalt–iron oxides, and a key factor is the presence of Co^{II} ions on the octahedral lattice sites, which can initiate a cyclic electron transfer process (redox reaction) on the catalyst surface.

Maximum activity, and lowest activation energy for the reaction, occurs at $x = 1$, since the greatest availability of octahedral Co^{II} occurs at this composition.

INTRODUCTION

The cobalt–iron spinel oxide system may be represented by the general formula $Co_xFe_{3-x}O_4$, where x, the composition variable, can take values between 0 and 3. This system was reported by Cota, Katan, Chin, and Schoenweis (*1*) to possess activity for hydrogen peroxide (H_2O_2) decomposition in alkaline solution comparable to highly active catalysts for the reaction such as silver and platinum black, when tested under similar conditions. The pronounced activity may be explained in terms of intrinsic factors, such as the chemical and electronic structures of the catalysts, or through microstructural factors, such as the surface area characteristics of the catalysts (*2*). The present paper describes an investigation of H_2O_2 decomposition by cobalt–iron spinel oxides in which intrinsic and microstructural factors are taken into account.

EXPERIMENTAL

In order to investigate H_2O_2 decomposition kinetics as a function of catalyst composition and microstructure, it was necessary to synthesize cobalt–iron oxides over the complete composition range of the system $(0 < x < 3)$, with differing surface areas. Two series were accordingly prepared. The first, consisting of high surface area powders, was obtained by hydroxide coprecipitation, using a method based on the work of Sato, Sugihara, and Saito (*3*). The second, a low surface area series, was prepared by the oxalate co-precipitation method of Schuele and Deetscreek (*4*). The two series of catalysts, prepared with x values of 0, 0.6, 1.0, 1.5, 2.0, 2.4, and 3.0,

are henceforth referred to as "hydroxide route" and "oxalate route" catalysts. The preparation of these oxides, their chemical characterization by X-ray and quantitative analysis, and their electronic structural analysis, revealing an inverse/normal structural change with composition, has been described elsewhere (*4–6*). These studies showed that the cobalt–iron oxides produced by the two routes possess similar crystal structure and chemical composition.

The activity of the catalysts towards H_2O_2 was evaluated in the liquid phase, using the gasometric technique of Cota *et al.* (*1*). Catalyst samples were injected into a stirred, thermostatted reaction vessel containing known volumes of reaction medium (usually KOH solution) and H_2O_2 solution. The weight of catalyst and the concentrations of the KOH and H_2O_2 solutions were accurately known. The KOH solution was freshly made up from carbonate-free Analar grade KOH pellets (Hopkin and Williams Ltd.) and the H_2O_2 solution from Laporte stabilizer-free 86% w/v H_2O_2, using deionized, distilled water. Both solutions were standardized immediately before runs, the KOH using standard HCl ampoules and the H_2O_2 using standard $KMnO_4$.

Oxygen was evolved from the reaction vessel according to the equation,

$$2HO_2^- = O_2 + 2OH^-, \qquad (1)$$

the H_2O_2 being present in alkaline solution as the perhydroxyl ion, HO_2^-. The oxygen evolution rate was monitored for a given temperature and atmospheric pressure, the oxygen displacing water from a Bunte gas burette. The results were corrected for self-decomposition of the H_2O_2, and the effect on the reaction kinetics of varying the catalyst mass, the H_2O_2 or KOH concentration, and the reaction temperature were investigated for the two catalyst series. The oxygen evolution rate was found to be independent of stirring.

The catalyst microstructures were characterized by visual investigation using a high resolution optical microscope and by surface area measurements. The BET specific surface areas were measured using nitrogen adsorption at −193°C, after initial degassing of the catalysts at 300°C for an hour. In addition, the catalyst samples were sent for particle sizing to Coulter Counter Ltd., Dunstable. For the particle sizing the oxide powders were ultrasonically dispersed in an isotonic aqueous electrolyte (0.1 *N* dibutyl phthalate) and evaluated as to mean aggregate size by Coulter counter analysis (*7*).

Two experiments were performed to assess whether the results on aggregate size distribution as measured by Coulter counter analysis are similar to the aggregate size distribution when the cobalt–iron oxides are used in the H_2O_2 decomposition apparatus. Coulter counter results for powders which have been used once in H_2O_2 activity tests gave similar aggregate size distribution results when subjected to Coulter counter analysis. Furthermore, the results for H_2O_2 decomposition when the tests were performed in an ultrasonic bath are the same as normal tests (i.e., the use of a magnetic stirrer). These experiments showed that the aggregates were quite

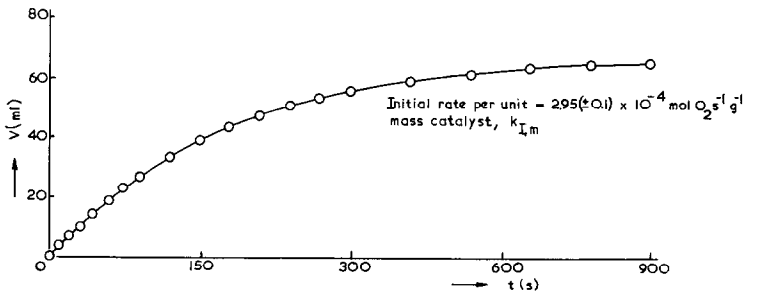

FIG. 1. *V–t* plot for H_2O_2 decomposition by hydroxide route $Co_1Fe_2O_4$ at 25°C.

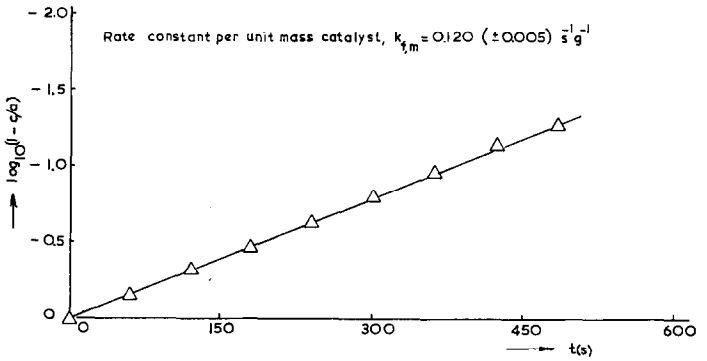

FIG. 2. $\text{Log}_{10}(1 - C/a)$ vs t plot, showing first-order kinetics, for H_2O_2 decomposition by hydroxide route $Co_1Fe_2O_4$.

firmly held together and that the results obtained from the Coulter counter analysis were reliable.

RESULTS

Hydroxide Route Catalysts

A plot of oxygen evolved vs time obtained for a reaction mixture of hydroxide route $Co_1Fe_2O_4$ (50.0 mg), 5 N KOH (50.0 ml), and 1.00 M H_2O_2 (5.0 ml) at 25.0 (±0.1)°C and one atmosphere pressure is shown in Fig. 1. V is the volume (ml) of oxygen evolved from the reaction mixture, while t(sec) is the time elapsed; the plot is corrected for self-decomposition of H_2O_2 (O_2 evolution rate at 25°C = 1.3 × 10^{-4} ml sec^{-1}). Figure 1 is typical of results obtained for hydroxide route catalysts.

The H_2O_2 decomposition kinetics for this series were found to follow a rate law which was first order with respect to H_2O_2. Thus, the results of Fig. 1 for hydroxide route $Co_1Fe_2O_4$, when expressed in the form of a $\log_{10}(1 - c/a)$ versus t plot, with a the initial concentration of H_2O_2 and c the concentration after time t, gave a linear plot (Fig. 2) over 95% of the total reaction time. In addition, the reaction rate constants were shown to be independent of the initial H_2O_2 concentration. These results are characteristic of first-order kinetics.

The first-order rate constants were also directly proportional to the catalyst mass in the reaction mixture, at least in the weight range 5–100 mg. In Fig. 3, the rate constant per unit mass catalyst, $k_{f,m}$, at 25°C, is plotted against x. The maximum error in $k_{f,m}$, values is ±5%. The effect of varying the reaction medium is demonstrated in Fig. 4, where the same reaction conditions as for Fig. 1 are maintained, with the exception of the reaction medium, which is changed successively from 5 N KOH to 10 N, 1 N, 0.1 N KOH, 10 N K_2CO_3, and distilled water (all 50 ml). In Fig. 4, $k_{f,m}$ at 25°C is plotted vs the reaction medium pH before H_2O_2 addition, measured either with a glass electrode pH

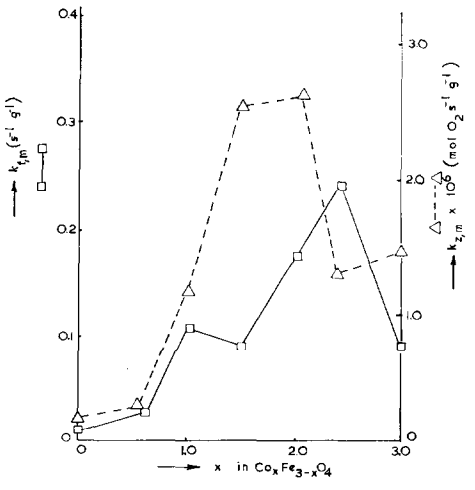

FIG. 3. Plot of $k_{f,m}$ (hydroxide route catalysts) and $k_{z,m}$ (oxalate route catalysts), at 25°C, as a function of x.

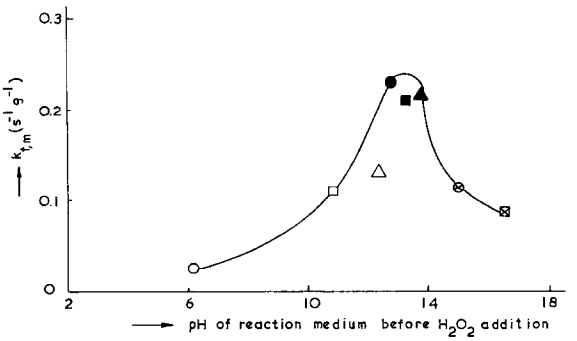

FIG. 4. Variation of $k_{f,m}$, at 25°C, with pH of reaction medium before H_2O_2 addition, for hydroxide route $Co_1Fe_2O_4$. Open circle, water; open square, 0.01 N KOH, open triangle, 10 N K_2CO_3; closed circle, 0.1 N KOH; closed square, 0.5 N KOH; closed triangle 1 N KOH; circle with cross, 5 N KOH; square with cross, 10 N KOH.

meter (pH < 14) or by calculation from activity coefficients (pH > 14) (*8*).

The rate constants $k_{f,m}$ increased with temperature between 5° and 50°C in accordance with the Arrhenius equation. The activation energies for H_2O_2 decomposition by hydroxide route cobalt–iron oxides are plotted vs composition in Fig. 5; the error in activation energy is ±0.5 kcal $mole^{-1}$.

The microstructural features are summarized in Table 1 and Fig. 6, which show, respectively, the BET specific surface area and mean aggregate size, d, of the catalysts as a function of x. The error in these parameters, as found by successive determinations, was ±5%.

Oxalate Route Catalysts

In contrast to V–t plots for hydroxide route catalysts, the V–t plots for oxalate route catalysts were linear. Figure 7 shows the V–t plot for oxalate route $Co_1Fe_2O_4$ obtained with similar conditions to Fig. 1, but with 250 mg catalyst. The plot is corrected for self-decomposition of H_2O_2. A linear V–t plot is indicative of reaction kinetics which are zero order with respect to H_2O_2. The zero-order rate constant, k_z, is then identical with the slope of the V–t plot. The rate constant was found to be directly proportional to the catalyst mass used in the reaction mixture, and in Fig. 3, the rate constant per unit mass of catalyst,

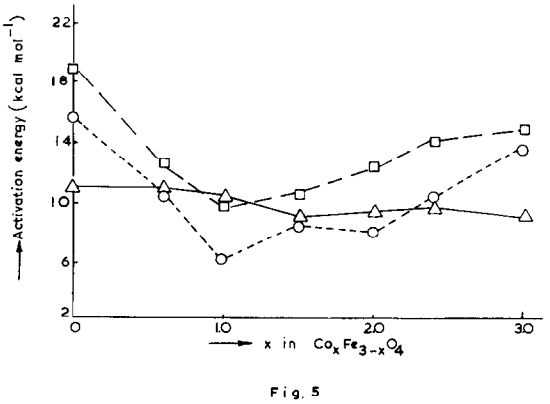

FIG. 5. Activation energy for H_2O_2 decomposition vs x: △, from $k_{f,m}$ values for hydroxide route catalysts; □, from $k_{z,m}$ values for oxalate route catalysts; ○, from $k_{I,m}$ values for hydroxide route catalysts.

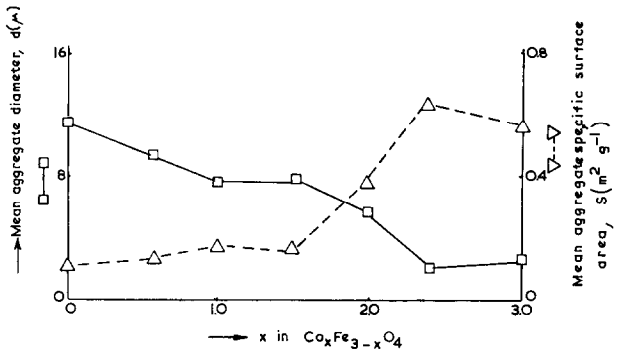

FIG. 6. Coulter counter measurements on hydroxide route catalysts: Mean aggregate diameter, (d), and mean aggregate specific surface area, (S), as a function of x.

$k_{z,m}$, at 25°C, is plotted vs x. The error in $k_{z,m}$ values was found to be ±5%. As observed for the hydroxide route series $k_{z,m}$ values increased with temperature in accordance with the Arrhenius equation. In Fig. 5 the activation energies for H_2O_2 decomposition are plotted vs x for the oxalate route series; activation energies were subject to ±0.5 kcal mole^{-1} error.

The BET specific surface area measurements on the oxalate route catalysts were all in the range 1–2 m^2 g^{-1}; since the error margin was large (±50%) for such small surface areas, it was impossible to arrange the catalysts in order of increasing surface area. The mean aggregate sizes are shown as a function of composition in Fig. 8; the error, as for the hydroxide route catalysts, was ±5%.

Analysis of Results

A key objective in the analysis of the reaction kinetics was to arrive at an intrinsic order of catalyst activities for

TABLE 1
PROPERTIES OF COBALT–IRON OXIDES[a]

Composition	Cation distribution and valency in the tetrahedral and octahedral sites of the spinel structure	BET specific surface area (±5%) m^2 g^{-1}	Activation energy for electronic conduction (±0.05 eV) eV	Theoretical density ρ (X-ray measurements) g cm^{-3}
A	Inverse			
$Co_0Fe_3O_4$	$(Fe_1^{III})_{tet}[Fe_1^{II}Fe_1^{III}]_{oct}O_4^{2-}$	130	0.10	5.22
B				
$Co_{0.6}Fe_{2.4}O_4$	$(Fe_1^{III})_{tet}[Co_{0.6}^{II}Fe_{0.4}^{II}Fe_{0.6}^{III}]_{oct}O_4^{2-}$	125	0.15	5.32
C	Inverse			
$Co_1Fe_2O_4$	$(Fe_1^{III})_{tet}[Co_1^{II}Fe_1^{III}]_{oct}O_4^{2-}$	90	0.34	5.30
D				
$Co_{1.5}Fe_{1.5}O_4$	$(Co_{0.5}^{II}Fe_{0.5}^{II})_{tet}[Co_{0.5}^{II}Co_{0.5}^{III}Fe_{1.0}^{III}]_{oct}O_4^{2-}$	85	0.27	5.52
E	Normal			
$Co_2Fe_1O_4$	$(Co_1^{II})_{tet}[Co_1^{III}Fe_1^{III}]_{oct}O_4^{2-}$	80	0.35	5.69
F				
$Co_{2.4}Fe_{0.6}O_4$	$(Co_1^{II})_{tet}[Co_{1.4}^{III}Fe_{0.6}^{III}]_{oct}O_4^{2-}$	75	0.44	5.80
G	Normal			
$Co_3Fe_0O_4$	$(Co_1^{II})_{tet}[Co_2^{III}]_{oct}O_4^{2-}$	60	0.52	6.07

[a] From ref. (*6*).

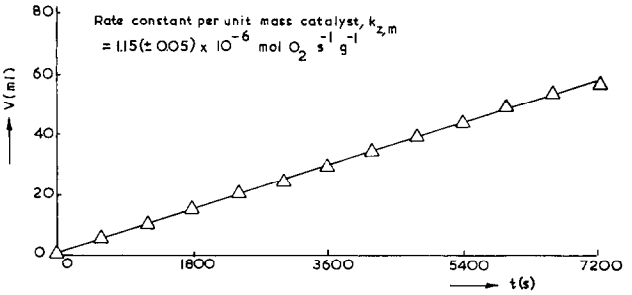

FIG. 7. V–t plot for H_2O_2 decomposition by oxalate route $Co_1Fe_2O_4$ at 25°C.

cobalt–iron oxides in H_2O_2 decomposition, one far more dependent on catalyst composition than microstructural differences. A comparison of the $k_{f,m}$ vs x plot for the hydroxide route catalysts with the $k_{z,m}$ vs x plot for the oxalate route catalysts (Fig. 3) indicates two main features. Under similar conditions the high surface area hydroxide route catalysts are nearly three orders of magnitude more active for H_2O_2 decomposition than the low surface area oxalate route catalysts. However, the variation of activity with composition is completely different for the two series, indicating that microstructural effects are operating within one, if not both, of the series.

One possible approach to ascertaining the intrinsic activity is to make use of a kinetic parameter which is effectively independent of the catalyst microstructure, for each member of the two series. A suitable choice for this parameter is the activation energy for the decomposition reaction, which is dependent on the catalyst type rather than its surface morphology (*9*). This approach could be checked by an independent analysis in which an attempt was made to normalize catalyst activities for microstructural differences. An important parameter characterizing catalyst microstructure might, for instance, be the BET specific surface area (*1*). In each series, the microstructure-independent parameter (activation energy) and the microstructure-normalized parameter (decomposition rate per unit surface area) should show similar intrinsic-only trends vs catalyst composition.

Activation Energies for H_2O_2 Decomposition

The activation energies for the hydroxide route catalysts, obtained from $k_{f,m}$ values, show little variation with catalyst composition (Fig. 5), being clustered in the range 9–11 kcal $mole^{-1}$. This result seemed unusual for a catalyst series with such pronounced differences in composition and

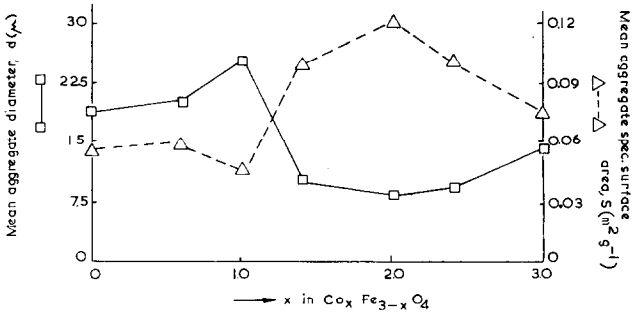

FIG. 8. Coulter counter measurements on oxalate route catalysts: Mean aggregate diameter, d, and mean aggregate specific surface area, S, as a function of x.

structure. Moreover, the oxalate route catalysts show a wide variation in activation energy with composition (9–19 kcal mole^{-1}, Fig. 5, from $k_{z,m}$ values), with a pronounced minimum at the composition $x = 1$.

The anomaly may be explained in terms of diffusion effects. With the hydroxide route catalysts the high reaction rate for oxygen evolution produced marked turbulence; in fact, the reaction rate was independent of mechanical stirring. However, when turbulence occurs near the surface of a solid dispersed in a liquid, a thin liquid layer, of thickness about 10 μm, adheres to the solid surface (*10*). For H_2O_2 decomposition by 3-phase heterogeneous catalysts, fresh H_2O_2 must diffuse through such a layer to the catalyst surface to maintain the reaction, and diffusion control may well control the overall decomposition kinetics (*11*).

The observed first-order rate law for the hydroxide route catalysts was thus the diffusion law for the H_2O_2 under the experimental conditions. With increasing mass of catalyst there would be more particles round which diffusion layers could be set up, explaining the dependence of the rate constant on the catalyst mass. Since the diffusion kinetics would be largely independent of catalyst composition, activation energies from $k_{f,m}$ values would be similar, as observed.

In order to verify this reasoning, the activation energies for the hydroxide route catalysts were obtained using initial rates per unit mass catalyst $k_{I,m}$ as a function of temperature. The $k_{I,m}$ values are less diffusion controlled than $k_{f,m}$ values, because in the initial stages of the reaction there elapses a finite time before the diffusion layer is set up; inevitably $k_{I,m}$ values are rather less accurate than $k_{f,m}$ ones due to the uncertainties in tangent drawing. The $k_{I,m}$ values, expressed in the units mole O_2 sec^{-1} g^{-1}, were subject to an error of $\pm 10\%$. The activation energies for the hydroxide route catalysts, based on $k_{I,m}$ values, are plotted vs cobalt–iron oxide composition in Fig. 5; the maximum error is of the order of ± 1 kcal mole^{-1}. This plot shows similar trends to the corresponding one for the oxalate series; thus, the activation energies for H_2O_2 decomposition vary from 6–16 kcal mole^{-1}, and there is again a pronounced minimum at the composition $x = 1$.

In the case of the oxalate route catalysts, the surface reaction rate is too slow to permit diffusion control. Zero-order kinetics can occur when the active centers at the catalyst surface are saturated with reactant, as found by Bagg for H_2O_2 decomposition on a silver crystal (*12*). The observed rates are hence a measure of the ease with which each catalyst clears H_2O_2 from its active centers, and activation energies derived from $k_{z,m}$ values are relatively diffusion-free and independent of microstructure.

The catalyst activities in the two series may be compared on the basis that the most effective H_2O_2 decomposition catalyst possesses the lowest activation energy. For the hydroxide route catalysts, the activity order, considering x values, is

$$1.0 > 2 \approx 1.5 > 2.4 \approx 0.6 > 3.0 > 0 \quad (2)$$

and for the oxalate route catalysts,

$$1.0 > 1.5 > 2.0 > 0.6 > 2.4 > 3.0 > 0. \quad (3)$$

The similarity, within experimental error, of results for the two series is strong evidence that the activation energies represent true intrinsic catalytic activities.

Values for the pre-exponential factor, A, were obtained from each Arrhenius plot. A may be related (*13*) to the active site concentration on the catalyst surface or the entropy of adsorption of the reacting species; Bond (*14*) has shown how these catalyst properties may be inferred from the dependence of A on the activation energy for the reaction (compensation effect). In the present study an overall compensation effect holds; however, no coherent trend between individual A values and catalyst composition could be found. Presumably randomizing factors in the reaction system mask a simple interpretation of A values.

Surface Area Effects in H_2O_2 Decomposition

The cobalt–iron oxides consist of powders, individual particles of which are somewhat porous, possessing irregular and discontinuous surface structures. The surface is interrupted by cracks and pores giving access to subsurface porous regions. Clearly the total surface is much greater than if the particles were wholly solid and continuous. Catalytically active centers are distributed probably just as much in internal pores as on the catalyst outer surface. To normalize for microstructural effects, surface areas should accordingly be evaluated by a technique for the surface area contribution of the internal structure. Cota *et al.* (*1*) applied such reasoning to their H_2O_2 decomposition studies, normalizing decomposition rates to unit specific surface area of catalyst as determined by the nitrogen adsorption (BET) technique.

When the H_2O_2 decomposition rate constants for the hydroxide route catalysts were normalized to unit BET specific surface area, it was found that the normalizing procedure had left largely unaffected the activity order represented by the original $k_{f,m}$ vs x plot, Fig. 3. Thus the trends in the normalized activity plot bore no resemblance to the intrinsic order shown in Fig. 5. No corroborative normalizing procedure could be carried out for the low surface area oxalate route catalysts, in view of the limitations in BET measurement accuracy. Nevertheless, the suggestion of Cota *et al.* that normalizing H_2O_2 decomposition rates to unit BET specific surface area yields intrinsic catalytic activities found no confirmation in the present study.

An alternative approach to microstructural normalization is based on considering the amount of catalyst total surface actually used in liquid phase H_2O_2 decomposition. For porous, ultrafine catalysts, the greatest contribution to the BET surface area arises from the pore walls of the developed internal structure. In fact, the outer surface of the catalyst probably represents only a small fraction of the total surface. Now, consider the utilization of catalyst internal surface in liquid phase H_2O_2 decomposition. To react over this region H_2O_2 must diffuse into and along the catalyst internal pores. However, the decomposition reaction is a turbulent process, continuously releasing bubbles of oxygen gas. Such a process, occurring in confined, subsurface pores would inevitably force out reactant solution, curtailing further decomposition.

According to this proposal, liquid phase H_2O_2 decomposition is greatly restricted in catalyst internal pores and occurs predominantly on the outer surface. Normalizing to unit BET specific surface area, largely a measure of internal surface, hence does not correct for the effect of catalyst microstructures on decomposition rates. Conversely, if a suitable parameter describing the outer surface area of the catalysts were measured, then normalizing decomposition rates for this outer surface area should yield an intrinsic measure of catalytic activity.

Using optical microscopy, the individual particles from both series were seen to be roughly spherical aggregates, with the effective diameter, rather than the overall shape, varying with composition. The aggregates, in the case of hydroxide route catalysts, possessed particle diameters generally in the range 1–10 μm, whereas the corresponding aggregates, in the case of the oxalate route catalysts, were much coarser, 10–50 μm diameter. The exposed portion of catalyst actually used in H_2O_2 decomposition would then be the outer surface of the aggregates. Assuming the aggregates to be approximated to by ideal spheres, then the mean aggregate specific surface area, S, is simply related to the mean aggregate diameter, d, of the spheres by the formula (*15*),

$$S = 6/d\rho$$

where ρ is the particle density.

The parameter d follows from the Coulter counter results (Figs. 6 and 8); ρ requires some knowledge of the aggregate densities. However, since the catalysts in each series were obtained by a similar coprecipitation/heat treatment procedure,

their porosities should be similar, and ρ can be taken to be the spinel theoretical density. Catalyst theoretical densities, obtained from X-ray data (*6*), are collected as a function of composition in Table 1.

Values of S are shown as a function of catalyst composition for hydroxide route catalysts in Fig. 6, and for oxalate route catalysts in Fig. 8. The error in S values, reflecting the variation in the d and ρ parameters used to derive S, is about $\pm 5\%$. Clearly, the absolute significance of the S parameter is questionable, in view of the limitations of the Coulter counter technique, and the approximations as to the ideal sphere nature and real density of the aggregates. Nevertheless, for a relative order of aggregate areas, the approach is adequate.

The initial rates per unit mass of catalyst, $k_{I,m}$ at 25°C, normalized to unit S values, are shown as a function of catalyst composition for both series in Fig. 9. The normalizing procedure is subject to a maximum error of $\pm 5\%$ error in Coulter counter measurements and the error of $\pm 10\%$ in $k_{I,m}$ values. Figure 9 exhibits significant differences from the $k_{I,m}$ vs x plot (Fig. 3). The order of activities, listing the x values, is for hydroxide route catalysts,

$$1.0 > 1.5 > 2.0 > 2.4 > 0.6 > 3.0 > 0 \quad (4)$$

and for the oxalate route catalysts,

$$1.0 > 1.5 > 2.0 > 3.0 > 2.4 > 0.6 > 0. \quad (5)$$

The activity orders (4) and (5) for the S-normalized rates are within experimental error fairly consistent with one another for the two series; they are also in agreement with the activity orders (2) and (3) derived for the two series on the basis of activation energies. Thus, overall in the four sequences (2)–(5) the greatest activity is shown for $x = 1$, and this is followed by the activities for $x = 1.5$ and 2.0. A third group follows, with $x = 2.4$ and 0.6, while the least active catalysts have $x = 3.0$ and 0.

The above results imply, firstly, that the mean aggregate specific surface area is a key parameter in assessing catalyst microstructures for H_2O_2 decomposition studies. Thus, S-normalized rates themselves represent intrinsic catalytic activities, since they agree with the intrinsic order derived from activation energies. This correlation from independent approaches is itself good evidence for intrinsic activity. Secondly, the results justify the use of Coulter counter analysis to compare catalyst aggregate surface areas, and the accompanying assumptions.

Mode of Operation of Cobalt–Iron Oxides in H_2O_2 Decomposition

A comparison of activation energy measurements and microstructure-normalized rates for H_2O_2 decomposition by cobalt–iron oxides from the hydroxide and oxalate routes has enabled an order representing catalyst intrinsic activities to

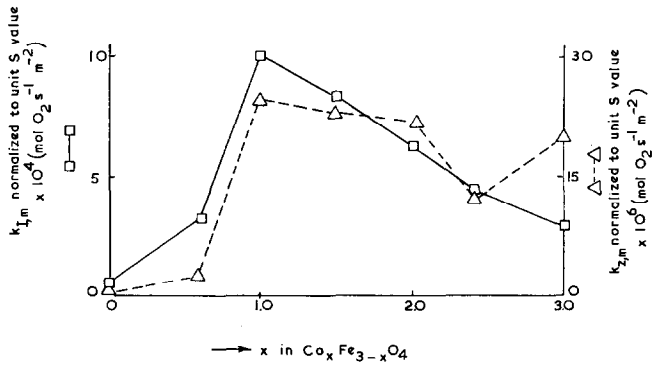

FIG. 9. Initial H_2O_2 decomposition rate at 25°C, normalized to limit mean aggregate specific surface area, S, as a function of x. □—□, hydroxide route catalysts; △- - -△, oxalate route catalysts.

be established. The overall activity order, considering the x value in $Co_xFe_{3-x}O_4$, is

$$1.0 > 1.5 > 2.0 > 2.4 > 0.6 > 3.0 > 0.0. \quad (6)$$

The intrinsic factors governing H_2O_2 decomposition by cobalt–iron oxides must now be discussed, and the order (6) justified.

There have been several approaches to the study of heterogeneous H_2O_2 decomposition by metal oxide systems. Schwab and co-workers (*16*, *17*) investigated H_2O_2 catalysis by ferrites, and concluded that Fe^{II} ions on the spinel sublattices could act as active centers for the decomposition reaction. The most favorable position for Fe^{II} in the case of inverse ferrites was found to be the octahedral sites; clearly, the effective number of Fe^{II} ions was increased due to the octahedral sites; clearly, the effective number of Fe^{II} ions was increased due to the possibility of electron hopping with adjacent Fe^{III} ions (*18*). Hart and co-workers (*19*, *20*), in a series of vapor phase H_2O_2 decomposition studies, classified oxide catalysts on the basis of defect type. In general, p-type oxides were more active than n-type oxides for the decomposition reaction.

An electrochemical approach to H_2O_2 decomposition reactions was emphasized by Ardon (*2*). If a system exists in two oxidation states having a suitable redox potential so that the lower oxidation state can be oxidized by H_2O_2, and the higher state reduced by it, and both reactions proceed at a measurable rate, then the system will act as an H_2O_2 decomposition catalyst. Roy (*21*) correlated the H_2O_2 decomposition activity of several transition metal oxides with their measured redox potentials. The dual valence oxides with standard redox potentials considerably above the standard reduction potential, 0.68 V (*22*), for H_2O_2 oxidation,

$$O_2 + 2H^+ + 2e = H_2O_2 \quad (7)$$

were effective catalysts, whereas those oxides with low standard redox potentials were much less active.

Whereas Schwab *et al.* were mainly concerned with electronic factors in H_2O_2 decomposition, a different approach was described by Parravano (*23*). Sintered $Co_xFe_{3-x}O_4$ samples, in the composition range $0.9 < x < 1.1$, were evaluated for their activities in H_2O_2 decomposition, oxygen adsorption, and N_2O decomposition. The results were correlated with earlier work on isotopic exchange ($CO/^*CO_2$ and H_2/D_2) (*24*, *25*) for the same catalyst compositions. Parravano showed that the rates of reaction which took place under oxidizing conditions (H_2O_2, N_2O decomposition, and oxygen adsorption) had a maximum value at catalyst compositions near $x = 1$, whereas the rates of reactions which took place under reducing conditions ($CO/^*CO_2$ and H_2/D_2 exchange) had a minimum value at this composition.

A generalized picture of the surface phenomena during catalysis was presented. For reactions under oxidizing conditions a common stage is the loading of the spinel surface with oxygen by means of O_2, CO_2, H_2O_2. Thus, (*26*, *27*)

Spinel surface + oxygen donor = oxidized adsorption layer + defects on spinel surface + oxygen acceptor. (8)

Similarly, for processes occurring under reducing conditions, the unloading of oxygen from the spinel surface by means of an oxygen acceptor or reduced pressure represents the common stage.

Parravano's basic assumption was that the surface reactions took place by means of a mechanism in which orientation relationships between adsorbent and adsorption layer were kinetically important and determined the variation of rate with catalyst composition. This topochemical rate control was significant in the narrow composition range studied, since variation of catalyst structure with composition was minimal, and the site occupancy in the spinel was determined by the Co/Fe ratio. Accordingly maximum or minimum rates found for a given reaction should also be observed, at the same composition, for the other reactions Topochemical rate control from diffusion effects along and within the adsorption layer during the rate determining step. Accordingly, diffusion rates for

cationic defects in Eq. (8) were shown to be a minimum for the spinel composition $x = 1$ in oxidizing reactions, but a maximum for the composition $x = 1$ in reducing reactions.

Parravano's results (*23*) for H_2O_2 decomposition by cobalt–iron oxides are presented in Fig. 10, which shows values for $k_{f,m}$ (25°C) and activation energies as a function of catalyst composition. The significant feature of these results is that a maximum $k_{f,m}$ value, and minimum activation energy, were found near the composition $Co_1Fe_2O_4$, agreeing with the present study; in addition the kinetics of H_2O_2 decomposition were first order with respect to H_2O_2, as found for hydroxide route catalysts. The $k_{f,m}$ values for Parravano's catalysts were much smaller than $k_{f,m}$ values from the present study, considering the similarity of the test conditions. This reflects the low surface areas of Parravano's sintered powders and decreased H_2O_2 decomposition rates for catalysts screened in neutral, rather than alkaline solution. However, there is as much variation in catalyst activities for the narrow composition range $0.9 < x < 1.1$ studied by Parravano, as is found in the present study for the whole series, $0 < x < 3$, showing the dominant effect of topochemical factors over narrow composition ranges.

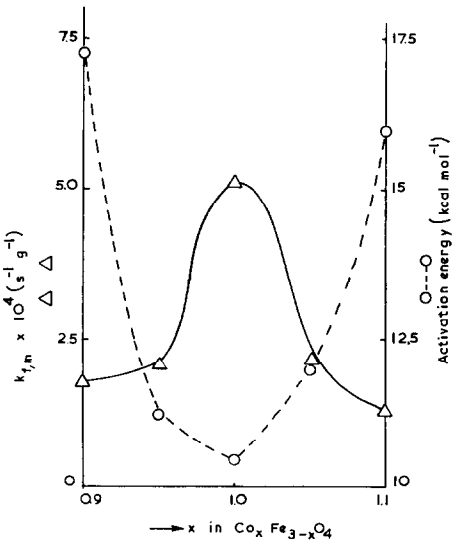

FIG. 10. H_2O_2 decomposition results of Parravano (*23*): $k_{f,m}$ values at 25°C, and activation energies, as a function of x, for sintered cobalt–iron oxides in 3×10^{-2} M aqueous H_2O_2.

The factors reviewed above may be considered in turn with respect to the cobalt–iron oxide system. The electronic structure and cation distribution of the system, established on the basis of conductivity measurements in a previous study (*6*), are presented as a function of composition in Table 1. Schwab *et al.* established the importance of Fe^{II}/Fe^{III} transitions on the spinel ferrite lattice as initiating centers for H_2O_2 decomposition. In the cobalt–iron oxide series, however, there are two types of divalent ion readily promoted to the trivalent state, Fe^{II} and Co^{II}. Co^{II}, as well as Fe^{II}, may act as catalytic centers for H_2O_2 decomposition.

The relative importance of Co^{II} and Fe^{II} centers may be gauged from the plots used to obtain the intrinsic activity order (6), viz., Figs. 5 and 9, for the two series. Clearly, Co_3O_4 possesses much greater intrinsic activity for H_2O_2 decomposition than Fe_3O_4. The electronic structures of Co_3O_4 and Fe_3O_4 are compositions G and A, respectively, in Table 1. The activity difference occurs despite the fact that all Fe^{II} in Fe_3O_4 is favorably positioned on octahedral sites, whereas all Co^{II} in Co_3O_4 is confined to tetrahedral sites. The Co^{II} centers in these spinels are thus much more effective than Fe^{II} centers for H_2O_2 decomposition.

An additional feature of the intrinsic activity plots is that Co_3O_4 is not drastically less active than the best catalysts in the cobalt–iron oxide system, whereas Fe_3O_4 is. This implies that activity enhancement through octahedral siting of catalytic centers is not so marked with Co^{II} in this system, as with Fe^{II} in the ferrite systems studied by Schwab and Kraut (*17*). This effect is related to the ease of octahedral site electron hopping on the spinel lattice as the ionic distribution changes. Conductivity measurements on the cobalt–iron oxide series showed (*6*) that electron exchange between Co^{II}/Co^{III} or

Co^{II}/Fe^{III} couples is much more restricted than Fe^{II}/Fe^{III} transfers.

The catalytic centers in cobalt–iron oxides may be arranged in order of decreasing intrinsic activity for H_2O_2 decomposition on the basis of the foregoing considerations. The most effective center is $(Co^{II})_{oct}$, with greater activity when the adjacent octahedral site ion is Co^{III} than when it is Fe^{III}. This follows from the electron hopping considerations. Both configurations afford somewhat greater activity than the case of $(Co^{II})_{tet}$, even when the adjacent species is $(Fe^{III})_{tet}$, due to the effective isolation of tetrahedral sites. However Co^{II}, wherever sited, is markedly superior to Fe^{II}, and Fe^{II} itself, when sited octahedrally with adjacent Fe^{III}, is superior to $(Fe^{II})_{tet}$. These principles may be schematically summarized:

$$[Co^{II} - Co^{III}]_{oct} > [Co^{II} - Fe^{III}]_{oct} > Co^{II}_{tet} \gg [Fe^{II} - Fe^{III}]_{oct} \gg (Fe^{II})_{tet}. \quad (9)$$

Considering the electronic structures in Table 1, the intrinsically most active catalyst should be C, with $x = 1$, since no other composition contains as much as 1 mole Co^{II} per formula weight on the octahedral sites. The next most active would be D, with $x = 1.5$. This, in common with E–G, has a total of 1 mole Co^{II} per formula weight, but only with D is as much as 50% of this Co^{II} octahedrally sited. Compositions E–G each have 1 mole Co^{II} tetrahedrally sited, and identical activity for H_2O_2 decomposition would be expected. However, over this composition range the activation energy for electronic conduction increases (*6*) (Table 1); this implies a drop in electron availability, and the H_2O_2 decomposition reaction, being an acceptor reaction, would respond such that the activity order became E > F > G. Composition G should itself be superior to B with $x = 0.6$, since although the Co^{II} in B is octahedrally sited, there is only 0.6 mole per formula weight. Finally composition B should be markedly superior to A, with $x = 0$, which possesses no Co^{II}, only Fe^{II}.

Hence the predicted intrinsic activity order is listing x values,

$$1.0 > 1.5 > 2.0 > 2.4 > 3.0 > 0.6 > 0. \quad (10)$$

This is in good general agreement with the observed activity order (6), derived on the basis of activation energies and microstructure-normalized rates. The only discrepancy is that the position of composition $x = 3$ and 0.6 in activity order (10) should be reversed. Clearly for these two compositions, there is a trade-off between the efficacy of a large amount of Co^{II} sited unfavorably (tetrahedrally in a poor electron donor system), and a smaller amount of Co^{II} sited favorably (octahedrally in a superior electron donor system).

The present study thus affords further support to the mechanism for H_2O_2 decomposition proposed by Schwab *et al.* based on divalent transition metal ions on spinel lattices. Moreover, the report of Hart *et al.* (*19*) that *p*-type semiconducting oxides were more active H_2O_2 decomposition catalysts than *n*-type, is confirmed here, since Jonker (*5*) showed that compositions with $x > 1$ in the system $Co_xFe_{3-x}O_4$ exhibited *p*-type semiconductivity, whereas those compositions with $x < 1$ were *n*-type semiconductors. Correspondingly, cobalt–iron oxides with $x > 1$ have H_2O_2 decomposition activities above those with $x < 1$.

The electrochemical approach of Roy (*21*) is supported also by this study, at least qualitatively. In alkaline solution the redox reactions of importance for the cobalt–iron oxide system,

$$Co(OH)_3 + e = Co(OH)_2 + OH^- \quad (11)$$

$$Fe(OH)_3 + e = Fe(OH)_2 + OH^- \quad (12)$$

have standard reduction potentials respectively, of +0.17 V and −0.56 V (*22*).

In comparing these values with the standard reduction potential, −0.08 V (*22*), for perhydroxyl ion oxidation,

$$O_2 + H_2O + 2e = HO_2^- + OH^- \quad (13)$$

it may be deduced that the couple (11) will be much more active for H_2O_2 decomposition than the couple (12). Inevitably, the redox species involved in the reaction at high pH levels on the spinel surface are less well characterized than (11) or (12)

would imply, precluding more quantitative predictions. However, Pourbaix (*28*) has reported that H_2O_2 can act as an oxidizing agent, converting CoO into Co_2O_3, and as a reducing agent, bringing about the reverse process; a state of equilibrium between the two oxides is reached. This would support the redox classification (*2*).

The importance of pH effects may be analyzed at this point. As shown in Fig. 4, a typical hydroxide route catalyst has a pronounced activity for H_2O_2 decomposition in neutral solution; the activity rises with increasing pH to a maximum at about pH 13–14 for KOH and drops sharply as the KOH concentration is increased further. The increase in rate with alkalinity of reaction medium has been observed for many H_2O_2 decomposition catalysts. The effect is attributed to the intrinsic instability of H_2O_2 in alkaline solution, and base catalysis by OH^- ions (*29*), but another factor is that reaction intermediates, such as oxide or hydroxide layers produced at catalyst surfaces during the decomposition reaction, become stabler at higher pH levels (*30*). The observed rate maximum near pH 14 has been observed for spinel catalysts similar in type to cobalt–iron oxides (*31*) and occurs even in the absence of heterogeneous catalysts (*9*, *31*). At very high KOH concentrations, transport of reactive species concerned with H_2O_2 decomposition is restricted and the rate should drop. Thus, the O_2 solubility and diffusion coefficient decrease with increasing KOH concentration (*32*), while the viscosity increases (*8*). An activity maximum at a high pH is thus justified for KOH solution.

Topochemical factors must also be considered in their effect on intrinsic catalytic activities. Parravano's work on cobalt–iron oxides was restricted to a narrow composition range $0.9 < x < 1.1$, thereby minimizing chemical variation and structural distortion within the lattice, and allowing kinetic control by reactant/adsorbent orientation to predominate. In the present study over the complete composition range, $0 < x < 3$, there are large overall chemical and structural changes, and the significance of topochemical effects will inevitably decrease.

Parravano did not evaluate electronic effects, but these may be important, since for $Co_xFe_{3-x}O_4$ in the composition range $0.9 < x < 1.1$ there are drastic changes in both conductivity (seven orders of magnitude) and thermoelectric power (-600 to $+800$ μV $°C^{-1}$) (*5*). It is, in fact, possible to explain Parravano's results on the basis of electronic structural differences. By interpolation from Table 1, the structure of $Co_xFe_{3-x}O_4$ for two compositions near $x = 1$, such as $x = 0.9$ and 1.1, would be, respectively,

$$(Fe^{III}_{0.1})_{tet}[Fe^{II}_{0.1}Fe^{III}_{1.0}Co^{II}_{0.9}]_{oct}O^{2-}_4 \quad (13)$$

$$(Co^{II}_{0.1}Fe^{III}_{0.9})_{tet}[Co^{II}_{0.9}Co^{III}_{0.1}Fe^{III}_{1.0}]_{oct}O^{2-}_4. \quad (14)$$

This is to be compared with the structure, for $x = 1$, of

$$(Fe^{III}_{1.0})_{tet}[Fe^{III}_{1.0}Co^{II}_{1.0}]_{oct}O^{2-}_4 \quad (15)$$

Oxidizing reactions, of which H_2O_2 decomposition is exemplary, respond to Co^{II}, especially on octahedral sites. The rate is hence a maximum for composition (15). Reducing reactions, as Schwab *et al.* (*16*) found for the CO/CO_2 reaction, respond to Fe^{III} only on tetrahedral sites. Octahedrally sited Co^{III} is also catalytically active for reducing reactions (*33*). A minimum in the rate should therefore result for such reactions at composition 15.

Conclusions

Similar trends in liquid phase H_2O_2 decomposition activity vs cobalt–iron oxide composition have been demonstrated for (i) a microstructure-independent kinetic parameter, viz., the diffusion-free activation energy, and (ii) a microstructure-normalized kinetic parameter, viz., the decomposition rate normalized to the catalyst mean aggregate specific surface area. This affords strong evidence that the observed trend represents the true intrinsic catalytic activity for the system. In addition, the results indicate that predominantly the outer aggregate surface of an ultrafine, porous H_2O_2 decomposition catalyst is effective in the decomposition reaction, with

the internal pore area correspondingly less important.

The decisive factors affecting intrinsic H_2O_2 decomposition activities by cobalt–iron oxides may finally be summarized. The major controlling factor is the electronic structure of the spinel. The occurrence of Co^{II} on octahedral sites, with its ready conversion to Co^{III}, allows a highly effective redox system to be set up, initiated by Co^{II} centers. However, catalysis control by topochemical or pH effects are not thought to be as important over the composition range and reaction conditions investigated.

ACKNOWLEDGMENT

This work was supported by the Science Research Council.

REFERENCES

1. COTA, H. M., KATAN, J., CHIN, M., AND SCHOENWEIS, F. J., *Nature (London)* **203**, 1281 (1964).
2. ARDON, M., "Oxygen," Sec. 4.4, pp. 91, 94. Benjamin, New York, 1965.
3. SATO, T., SUGIHARA, M., AND SAITO, M., *Rev. Elec. Comm. Lab.* **11**, 26 (1963).
4. SCHUELE, W. J., AND DEETSCREEK, V. D., *in* "Ultrafine Particles" (W. E. Kuhn, Ed.), p. 224. Wiley, New York and London, 1963.
5. JONKER, G. H., *J. Phys. Chem. Solids* **9**, 165 (1965).
6. TSEUNG, A. C. C., AND GOLDSTEIN, J. R., *J. Mat. Sci.* **7**, 1383 (1972).
7. ALLEN, T., "Particle Size Measurement," Chap. 10, p. 143. Chapman and Hall, London, 1968.
8. UNO FALK, S., AND SALKIND, A. J., "Alkaline Storage Batteries," Chap. 8, pp. 599, 588. Wiley, New York and London, 1969.
9. SCHUMB, W. C., SATTERFIELD, C. N., AND WENTWORTH, R. L., "Hydrogen Peroxide," Chap. 8, pp. 472, 476. Reinhold, New York, 1955.
10. WILLIAMS, K. R., "An Introduction to Fuel Cells," Chap. 3, p. 38. Elsevier, London, 1966.
11. PANNETIER, G., AND SOUCHAY, P., "Chemical Kinetics," Chap. 9, p. 410. Elsevier, London, 1967.
12. BAGG, J., *Austral. J. Chem.* **15**, 201 (1962).
13. HART, A. B., AND ROSS, R. A., *J. Catal.* **2**, 121 and 251 (1963).
14. BOND, G. C., "Catalysis by Metals," Chap. 7, p. 139. Academic Press, New York, 1962.
15. ORR, JR., C., AND DALLAVILLE, J. M., "Fine Particle Measurement," Chap. 2, p. 26. Macmillan, New York, 1959.
16. SCHWAB, G. M., ROTH, E., GRINZOS, CH., AND MAVRAKIS, N., *in* "Structure and Properties of Solid Surfaces" (R. Gomer and C. S. Smith, Eds.), Chap. 14, p. 464. Univ. of Chicago Press, Chicago, 1953.
17. SCHWAB, G. M., AND KRAUT, A., *Z. Anorg. allgem. Chem.* **295**, 36 (1958).
18. SUCHET, J. P., "Chemical Physics of Semiconductors" (trans. E. Heasell), Chap. 5, pp. 82, 83. Van Nostrand, London, 1965.
19. HART, A. B., MCFADYEN, J., AND ROSS, R. A., *Trans. Faraday Soc.* **59**, 1458 (1963).
20. HART, A. B., AND ROSS, R. A., *Nature (London)*, **193**, 1175 (1962).
21. ROY, C. B., *J. Catal.* **12**, 129 (1969).
22. LATIMER, W. M., "Oxidation Potentials," 2nd. ed., Appendix 1, pp. 343, 347. Prentice-Hall, New Jersey, 1952.
23. PARRAVANO, G., *Proc. of the 4th Int. Congress on Catalysis* (Moscow, 1968), Vol. I, p. 149 (Paper 11). Akademiai Kiado, Budapest, 1971.
24. HUANG, C. R., Ph.D. Thesis, 1966, Univ. of Michigan, Ann Arbor, Michigan.
25. SQUIRES, R. G., AND PARRAVANO, G., *J. Catal.* **3**, 324 (1963).
26. MULLER, W., AND SCHMALZRIED, H., *Ber. Bunsenges. Phys. Chem.* **68**, 270 (1964).
27. SCHMALZRIED, H., *in* "Progress in Solid State Chemistry" (H. Reiss, Ed.), Vol. 2, p. 265. Pergamon, London, 1965.
28. POURBAIX, M., "Atlas of Electrochemical Equilibria in Aqueous Solutions" (trans. J. A. Franklin), Chap. 4, p. 326. Pergamon, London, 1966.
29. DUKE, F. R., AND HAAS, T. W., *J. Phys. Chem.* **65**, 304 (1961).
30. MCKEE, D. W., *J. Catal.* **14**, 355 (1969).
31. KORDESCH, K., *in* "Fuel Cells" (W. Mitchell, Jr., Ed.), p. 340. Academic Press, London, 1963.
32. AUSTIN, L. G., *in* "Handbook of Fuel Cell Technolcgy" (C. Berger, Ed.), pp. 144, 145. Prentice-Hall, New Jersey, 1968.
33. LINDE, V. P., MARGOLIS, L. YA., AND ROGZINSKII, S. Z., *Dokl. Akad. Nauk SSR* **136**, 860 (1961).